

## Catalytic mechanism of activated carbon-assisted bioleaching of enargite concentrate

Oyama, Keishi

Department of Earth Resource Engineering, Faculty of Engineering, Kyushu University

Shimada, Kazuhiko

Department of Earth and Planetary Sciences, Faculty of Science, Kyushu University

Ishibashi, Jun-ichiro

Department of Earth and Planetary Sciences, Faculty of Science, Kyushu University

Sasaki, Keiko

Department of Earth Resources Engineering, Faculty of Engineering, Kyushu University

他

<https://hdl.handle.net/2324/4737402>

---

出版情報 : Hydrometallurgy. 196 (105417), 2020-09. Elsevier

バージョン :

権利関係 :



Title:

Catalytic mechanism of activated carbon-assisted bioleaching of enargite concentrate

Keishi OYAMA<sup>a</sup>, Kazuhiko SHIMADA<sup>b</sup>, Jun-ichiro ISHIBASHI<sup>b</sup>, Keiko SASAKI<sup>a</sup>,  
Hajime MIKI<sup>a</sup>, Naoko OKIBE<sup>a\*</sup>

<sup>a</sup>Department of Earth Resources Engineering, Faculty of Engineering, Kyushu University,  
744 Motoooka, Nishi-ku, Fukuoka 819-0395, Japan

<sup>b</sup> Department of Earth and Planetary Sciences, Faculty of Science, Kyushu University,  
744 Motoooka, Nishi-ku, Fukuoka 819-0395, Japan

\*Corresponding author

Tel. and Fax: +81 92 802 3312

E-mail address: okibe@mine.kyushu-u.ac.jp (Naoko OKIBE)

**Keywords:** enargite concentrate; bioleaching; activated carbon; solution redox potential;  
kinetic modeling

## Abstract

The catalytic mechanism of activated carbon-assisted bioleaching of enargite concentrate (enargite 37.4%; pyrite 47.3%) was investigated by employing microbiological, electrochemical and kinetic studies. By using moderately thermophilic microorganisms at 45°C, the final Cu dissolution was improved from 36% to 53% at 0.2% (w/v) activated carbon. An excess activated carbon addition showed an adverse effect. The enargite mineral itself favored higher solution redox potential ( $E_h$ ) for solubilization. However, the dissolution of co-existing pyrite, which also favors high  $E_h$ , immediately hindered enargite dissolution through the passivation effect. The surface of activated carbon functioned as an electron mediator to couple RISCs oxidation and  $Fe^{3+}$  reduction, so that elevation of the  $E_h$  level was controlled by offsetting microbial  $Fe^{3+}$  regeneration. As long as the  $E_h$  level was suppressed at <700 mV, the dissolution of pyrite was largely avoided, enabling a steady and continuous dissolution of the enargite mineral through the surface chemical reaction model. When the  $E_h$ -control by activated carbon becomes no longer sustainable and the  $E_h$  hits 700 mV, rapid pyrite dissolution was initiated and the surface chemical reaction of enargite dissolution came to an end. Arsenic species dissolved from enargite was constantly immobilized with an efficiency of 75-90% as amorphous ferric arsenate. However, the sudden initiation of pyrite dissolution also triggered the re-solubilization of ferric arsenate. Therefore, the sustainable  $E_h$ -controlling effect was shown to be critical to enable longer Cu dissolution from enargite as well as stabilization of As precipitates.

## 1. Introduction

Enargite ( $\text{Cu}_3\text{As}^{\text{V}}\text{S}_4$ ) is a highly refractory primary copper sulfide containing toxic arsenic. In order to scavenge the Cu value from enargite with the drawback of this toxic impurity, bioleaching is considered one of the most promising technologies from its environmental and economic advantages.

High-temperature bioleaching (65-70°C) was generally shown to be effective in several studies, achieving the final Cu dissolution ranging 52-91% (Escobar et al., 2000; Muñoz et al., 2006; Lee et al., 2011; Takatsugi et al., 2011). However, the effect largely drops when low-temperatures (25-30°C) are used (<15%; Escobar et al., 1997; Sasaki et al., 2010) and thereby necessity of reaction catalyst is stressed to improve the reaction. Hence, to overcome the refractoriness of enargite, several studies (incl. chemical leaching, electrochemical and bioleaching studies) aimed to search the effect of catalysts such as silver (Ag) and carbon materials.

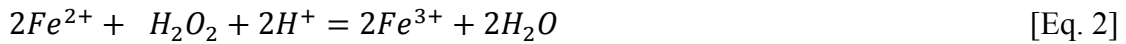
The utility of the Ag catalyst has been recognized in the case of another refractory primary copper sulfide mineral, chalcopyrite ( $\text{CuFeS}_2$ ), in both bioleaching studies (Ahonen and Tuovinen et al., 1990; Muñoz et al., 2007) and chemical leaching studies (Hiroyoshi et al., 2002; Nazari et al., 2012a, 2012b; Ghahremaninezhad et al., 2015; Nazari et al., 2011).

More recently, the catalytic effect of Ag was also confirmed with enargite in an electrochemical study, where the presence of Ag was suggested to promote the transformation of enargite into more amenable intermediate, chalcocite ( $\text{Cu}_2\text{S}$ ), at the specific  $E_h$  range (Miki et al., 2016). Furthermore, Oyama et al. (2018) suggested that the mechanism of Ag-catalyzed bioleaching of enargite concentrate proceeds via at least two types of intermediates (i.e.,  $\text{Cu}_2\text{S}$  and trisilver arsenic sulfide ( $\text{Ag}_3\text{AsS}_4$ )).

To alternate the expensive Ag catalyst, the effect of carbon has been also a focus of bioleaching as well as (electro)chemical leaching studies. In the case of chalcopyrite,

the effectiveness of activated carbon in bioleaching was reported, where the galvanic interaction between electrically nobler activated carbon and electrically poorer chalcopyrite, as well as the lowered  $E_h$  level, were suggested to be the driving force for the mineral dissolution (Nakazawa et al., 1998; Zhang et al., 2007; Liang et al., 2010; Ma et al., 2017; Hao et al., 2018).

As for the case of enargite, Olvera et al. (2013) performed electrochemical studies and proposed that the catalytic effect of activated carbon is caused by its role such as a conducting channel, an extension of the surface area for the reduction of  $O_2$  and  $Fe^{3+}$  and as a modifier of the semiconducting properties of the mineral. Ahumada et al. (2002) reported that the catalytic effect of activated carbon on chemical enargite leaching includes direct  $Fe^{2+}$  oxidation to  $Fe^{3+}$  by its surface oxygen groups as well as indirect  $Fe^{2+}$  oxidation via generation of  $H_2O_2$  from  $O_2$ , according to [Eq. 1] and [Eq. 2]:



Jahromi and Ghahreman (2016; 2019) conducted chemical enargite leaching studies and attributed the catalytic effect of CBCs (carbon-based catalysts) to the concentration of quinone-like functional groups.

Nonetheless, the catalytic effect of activated carbon is yet poorly understood in the bioleaching reaction of enargite. The fundamental difference between the two representative primary copper sulfides, chalcopyrite and enargite, is that unlike the case of chalcopyrite leaching which favors the controlled  $E_h$  level (Hiroyoshi et al., 2008), the dissolution of the enargite mineral itself favors the strong oxidizing condition (Lattanzi et al., 2008). Therefore, the effect of activated carbon may be expressed differently between the two cases. In the case of As-bearing enargite, the presence of activated carbon may also affect the oxidation/immobilization reaction of As species during bioleaching, as was observed by Jahromi et al. (2018). Thus, this study aimed to evaluate the effect of

95    activated carbon on bioleaching of enargite concentrate and to elucidate its mechanism  
96    employing microbiological, electrochemical and kinetic modeling studies.  
97

## 2. Materials and methods

### 2.1. Microorganisms

For oxidative dissolution of As-bearing enargite and other sulfide minerals in this study, the following three bacterial strains were chosen: Fe-oxidizing *Acidimicrobium ferrooxidans* ICP<sup>T</sup> (DSM 10331); Fe/S-oxidizing *Sulfobacillus sibiricus* N1<sup>T</sup> (DSM 17363); S-oxidizing *Acidithiobacillus caldus* KU<sup>T</sup> (DSM 8584). This bacterial consortium was shown to be effective in the oxidative dissolution of arsenopyrite while releasing over 15 mM total As (Tanaka et al., 2015). The three strains were routinely cultivated aerobically in 500 mL Erlenmeyer flasks containing 200 mL of heterotrophic basal salts (HBS) medium (0.5 g/L MgSO<sub>4</sub>·7H<sub>2</sub>O, 0.45 g/L (NH<sub>4</sub>)SO<sub>4</sub>, 0.05 g/L KCl, 0.05 g/L KH<sub>2</sub>PO<sub>4</sub>, 0.014 g/L Ca(NO<sub>3</sub>)<sub>2</sub>·4H<sub>2</sub>O, 0.142 g/L Na<sub>2</sub>SO<sub>4</sub>; pH 1.5 with H<sub>2</sub>SO<sub>4</sub>). None of the three strains was shown to exhibit the obvious As(III) oxidation activity (Okibe and Fukano, 2019). For *Am. ferrooxidans* ICP and *Sb. sibiricus* N1, 0.02% (w/v) yeast extract plus 10 mM Fe<sup>2+</sup> (added as FeSO<sub>4</sub>·7H<sub>2</sub>O) were added. For *At. caldus* KU, 0.5 g S<sup>0</sup> plus 200 µL of trace elements stock solution (10 mg/L ZnSO<sub>4</sub>·7H<sub>2</sub>O, 1 mg/L CuSO<sub>4</sub>·5H<sub>2</sub>O, 1.09 mg/L MnSO<sub>4</sub>·5H<sub>2</sub>O, 1 mg/L CoSO<sub>4</sub>·7H<sub>2</sub>O, 0.39 mg/L Cr<sub>2</sub>(SO<sub>4</sub>)<sub>3</sub>·7H<sub>2</sub>O, 0.6 mg/L H<sub>2</sub>BO<sub>3</sub>, 0.5 mg/L Na<sub>2</sub>MoO<sub>4</sub>·2H<sub>2</sub>O, 0.1 mg/L NaVO<sub>3</sub>, 1 mg/L NiSO<sub>4</sub>·6H<sub>2</sub>O, 0.51 mg/L Na<sub>2</sub>SeO<sub>4</sub>, 0.1 mg/L Na<sub>2</sub>WO<sub>4</sub>·2H<sub>2</sub>O) were added. The flasks were incubated shaken at 150 rpm at 45°C.

### 2.2. Minerals

The enargite concentrate (P<sub>80</sub> = 90 µm) used in this study was from Peru, consisting of enargite (Cu<sub>3</sub>AsS<sub>4</sub>) 37.4% and pyrite (FeS<sub>2</sub>) 47.3%, with minor amounts of tennantite ((Cu,Fe)<sub>12</sub>As<sub>4</sub>S<sub>13</sub>), chalcopyrite (CuFeS<sub>2</sub>), sphalerite (ZnS), stibnite (Sb<sub>2</sub>S<sub>3</sub>) and quartz (SiO<sub>2</sub>) (JX Nippon Mining & Metals). The elemental composition of enargite concentrate was as follows; S 39%, Fe 22%, Cu 20%, As 7.1%, Zn 0.39%, Sb 0.32%, Al

0.22%. Prior to the bioleaching experiment, the enargite concentrate was washed with 1 M HNO<sub>3</sub>, deionized water and ethanol.

### 2.3. Activated carbon

Granular activated carbon (CAS RN: 7440-44-0; Wako) of the average particle size of 5 mm was used in this study. The BET (Brunauer, Emmett and Teller) specific surface area and average pore diameter of activated carbon were determined to be 1212 m<sup>2</sup>/g and 1.77 nm, respectively, according to the procedures described by Konadu et al. (2017).

### 2.4. Bioleaching tests

Pre-grown cells of each of the three strains were harvested by centrifugation (9000 rpm, 10 min at 4°C) and washed twice with acidified water (pH 1.7), prior to inoculation into 200 mL HBS medium (pH 2.0; in 500 mL Erlenmeyer flasks) containing 2% (w/v) enargite concentrate and 5 mM Fe<sup>2+</sup> (so as to set the initial cell density of each strain at 1.0 × 10<sup>7</sup> cells/mL). Activated carbon was added into the medium at different concentrations; 0, 0.1, 0.2 or 0.3% (w/v). Flasks were incubated shaken at 150 rpm and 45°C for 60 days. Samples were regularly withdrawn (immediately after vigorously mixing the flask to maintain the solid/liquid ratio) to monitor pH, E<sub>h</sub>, cell density and concentrations of Fe<sup>2+</sup>, total Fe, total As and total Cu.

### 2.5. Solution and solid analyses

Liquid samples were filtered (0.20 µm) to measure concentrations of total Cu, Fe and As by inductively coupled plasma optical emission spectrometry (ICP-OES; Optima 8300DV; PerkinElmer), and Fe<sup>2+</sup> by the *o*-phenanthroline method (Caldwell and Adams, 1946). Leaching residues were collected after the bioleaching test and freeze-



dried overnight for X-ray diffraction (XRD; Rigaku; Ultima IV; CuK $\alpha$  40 mA, 40 kV) analysis. For elemental composition analysis by electron probe microanalyzer (EPMA; JOEL; JXA-8530F; 6 nA, 20 kV), the leaching residues were embedded into resin and polished. The incident electron beam was focused to 1  $\mu$ m in diameter.

## 2.6. The catalytic activity of activated carbon

Abiotic tests: Activated carbon (0.1%) was added to 100 mL of acidophile basal salts (ABS) medium (0.5 g/L MgSO $_4$ ·7H $_2$ O, 0.45 g/L (NH $_4$ )SO $_4$ , 0.05 g/L KCl, 0.05 g/L KH $_2$ PO $_4$ , 0.014 g/L Ca(NO $_3$ ) $_2$ ·4H $_2$ O, 0.15 g/L Na $_2$ SO $_4$ ·10H $_2$ O; pH 2.0 with H $_2$ SO $_4$ ) in 300 mL Erlenmeyer flask. Different combinations of Fe $^{3+}$  (as Fe $_2$ (SO $_4$ ) $_3$ ·nH $_2$ O), Fe $^{2+}$  (as FeSO $_4$ ·7H $_2$ O), S $_4$ O $_6^{2-}$  (as Na $_2$ S $_4$ O $_6$ ·2H $_2$ O) and yeast extract were added to the flasks as follows: 10 mM Fe $^{3+}$  only; 10 mM Fe $^{2+}$  only; 5 mM S $_4$ O $_6^{2-}$  only; 10 mM Fe $^{3+}$  plus 5 mM S $_4$ O $_6^{2-}$ ; 10 mM Fe $^{3+}$  plus 0.02% yeast extract. Activated carbon-free control flasks containing 10 mM Fe $^{3+}$  plus 5 mM S $_4$ O $_6^{2-}$  were also set-up.

## 2.7. Real-time PCR

In order to investigate the microbial population structure in bioleaching cultures, purification of genomic DNA, PCR-amplification of the 16S rRNA gene (template for real-time PCR), purification of the resultant PCR products and Real-Time PCR (MiniOpticon, Bio-Rad) were conducted according to the methods described by Oyama et al. (2018), with the exception that species-specific primers for *Ferroplasma acidiphilum* were not used in this study. Conditions for PCR and Real-Time PCR were described by Tanaka et al. (2015).

## 2.8. Electrochemical measurement of galvanic interaction

Three mineral electrodes (1 cm $^3$  cube of enargite, pyrite or activated carbon)

were prepared and polished by emery-paper to provide a fresh flat surface before each measurement. Diluted H<sub>2</sub>SO<sub>4</sub> solutions (0.1 M) with varying  $E_h$  values (0.5, 0.53, 0.6, 0.68, 0.74, 0.8, 0.86 or 0.9 V (vs. SHE)) were prepared by adjusting the Fe<sup>2+</sup>/Fe<sup>3+</sup> ratio using 0.1 M Fe solutions. The  $E_h$  values were measured with the Ag/AgCl reference electrode and the Pt working electrode. The Pt electrode was then replaced with each of the mineral electrodes to measure mineral potentials ( $E_{En}$ ,  $E_{Py}$  and  $E_{Ac}$ , respectively, for 300 sec) using the electrochemical analyzer (1280C, Solartron Analytical). The  $\Delta E_{En-Ac}$  and  $\Delta E_{En-Py}$  values were defined as the galvanic electromotive force between the two minerals. The galvanic current between the two minerals ( $I_{En-Ac}$  or  $I_{En-Py}$ ) was measured (300 sec) by connecting the enargite electrode to either activated carbon electrode or pyrite electrode, by applying the Galvanic electromotive force ( $\Delta E_{En-Ac}$  or  $\Delta E_{En-Py}$ ) to simulate the galvanic interaction between the two minerals.

## 2.9 Kinetic calculation

The activated carbon-catalyzed bioleaching reactions were evaluated by the shrinking core model. Based on this model, the mineral particle dissolution proceeds via diffusion through liquid film [Eq. 3], diffusion through product film [Eq. 4] or surface chemical reaction [Eq. 5], as the rate-limiting step (Wadsworth and Sohn, 1979).

$$X = k_l t \quad [\text{Eq. 3}]$$

$$1 - 3(1 - X)^{2/3} + 2(1 - X) = k_d t \quad [\text{Eq. 4}]$$

$$1 - (1 - X)^{1/3} = k_r t \quad [\text{Eq. 5}]$$

X: the fraction of dissolved Cu

t: the reaction time (day)

k: the rate constant (day<sup>-1</sup>)

### 3. Results and Discussion

#### 3.1. Effect of the activated carbon dose on the dissolution of enargite concentrate and microbial population structure

Cell-free control cultures: In the absence of activated carbon, the low  $E_h$  level of <600 mV (Fig. 1d) suppressed both Cu dissolution (11% on day 60; Fig. 1a) and Fe dissolution (9% on day 60; Fig. 1b). At 0.3% activated carbon, the  $E_h$  level increased slightly (<620 mV; Fig. 1d), due to its chemical  $Fe^{2+}$ -oxidizing effect (Jahromi et al., 2019). This resulted in a slight increase in Cu dissolution (23% on day 60; Fig. 1a) and Fe dissolution (16% on day 60; Fig. 1b). In all cell-free controls (0% and 0.3% activated carbon), the data from Fig. 1c suggested that As dissolved from enargite was constantly immobilized with an efficiency of 75-90%.

Bioleaching cultures: In the absence of activated carbon, microbial  $Fe^{2+}$  oxidation readily progressed to increase the  $E_h$  level to >800 mV (on day 20; Fig. 1d, e), accompanied by the most extensive Fe dissolution (Fig. 1b) and the final Cu dissolution of 36% (Fig. 1a). The addition of activated carbon at 0.1% and 0.2% increasingly suppressed the  $E_h$  rise (Fig. 1d), which improved the final Cu dissolution (46% and 53%, respectively; Fig. 1a) while delaying the Fe dissolution (Fig. 1b). However, further increasing the activated carbon dose to 0.3% strongly suppressed the  $E_h$  level (<645 mV; Fig. 1d), which adversely affected the final Cu dissolution (35% on day 60; Fig. 1a). Unlike the case of chalcopyrite (Masaki et al., 2018), enargite leaching favors the strong oxidizing condition (i.e., higher  $E_h$ ) (Lattanzi et al., 2008). In fact, the initial Cu leaching rate (day 0-10) was the greatest without activated carbon, followed by with 0.1% and 0.2% activated carbon (Fig. 1a); this is in accordance with the order of the  $E_h$  level from higher to lower (Fig. 1d). However, as soon as the  $E_h$  level hits ~700 mV (Fig. 1d), dissolution of Fe from the pyrite mineral was boosted (Fig. 1b), as was also reported by Gu et al. (2012). This resulted in the rapid passivation of the enargite surface to slow

down the Cu dissolution rate (Fig. 1a). Therefore, the catalytic role of activated carbon is not directly attributed to the acceleration of enargite dissolution itself, but to suppression of pyrite dissolution by keeping the  $E_h$  level to  $<700$  mV for a longer period, which indirectly allows durable Cu dissolution without passivation (Fig. 1a). It can be calculated from Fig. 1c that As dissolved in all inoculated cultures was constantly immobilized with an efficiency of over 70%, as long as the  $E_h$  level kept below 700 mV (Fig. 1d). However, the sudden start of Fe dissolution from pyrite on day 10, 25 and 38 (at 0%, 0.1% and 0.2% activated carbon, respectively; Fig. 1b) not only halted further As immobilization but also induced re-solubilization of As precipitates so far formed (Fig. 1f).

EPMA elemental mapping of a bioleached enargite concentrate sample in Fig. 2 (0.2% activated carbon, collected on day 30) indicated that an enargite grain is covered with 1-7  $\mu\text{m}$ -thick secondary layer (Fig. 2a) composed of Fe, As and O, corresponding to ferric arsenate ( $\text{FeAsO}_4$ ). The timing of the initiation of the re-solubilization of this amorphous ferric arsenate (on day 10, 25 and 38 at 0, 0.1 and 0.2% activated carbon, respectively; Fig. 1f) coincided with a surge in the Fe concentration (i.e. pyrite dissolution) (Fig. 1b). Tanaka et al. (2018) reported that crystallization of scorodite ( $\text{FeAsO}_4 \cdot 2\text{H}_2\text{O}$ ) is preceded by the formation of  $\text{SO}_4^{2-}$ -bearing amorphous precursor mixture composed of basic ferric sulfate ( $\text{MFe}_x(\text{SO}_4)_y(\text{OH})_z$ ) and ferric arsenate ( $\text{FeAsO}_4 \cdot (2+n)\text{H}_2\text{O}$ ). These precursors repeatedly dissolve and re-crystallize until metal ions become locally concentrated to trigger scorodite mineralization. Based on this mechanism, the observation here can be explained that a sudden influx of  $\text{SO}_4^{2-}$  deriving from pyrite favored stabilization of basic ferric sulfate, rather than ferric arsenate, eventually leading to mineralization of jarosite rather than scorodite.

Cell growth at 0.1% activated carbon was mostly equivalent to that without activated carbon. However, increasing the activated carbon dose to 0.2% caused an apparent lag in total cell growth (Fig. 3a). Especially, the planktonic cell count was

significantly lowered at the highest activated carbon dose of 0.3% (Fig. 3a). The possible reason for this observation may include cell attachment on the activated carbon surface which physically inhibits cell replication and/or adsorption of nutrients onto the activated carbon surface possibly hindering the cell feeding on the activated carbon surface. However, the exact reason is yet unclear. The microbial population structure analysis by Real-Time PCR is shown in Fig. 3b. As was mentioned in our previous study (Tanaka et al., 2015), based on the known copy number of 16S rRNA genes per genome (i.e., 2 copies in *At. caldus* KU, Valdes et al., 2009; 2 copies in *Am. ferrooxidans* ICP, Clum et al., 2009; 3–5 copies in other *Sulfobacillus* spp., Anderson et al., 2012; Li et al., 2011; Travisany et al., 2012), the abundance of *Sb. sibiricus* N1 may be overestimated in this mixed culture. Therefore, it can be said that at the activated carbon dose of 0-0.2%, the major microbial components were *At. caldus* KU and *Am. ferrooxidans* ICP on both day 30 and day 60. The addition of activated carbon (up to 0.2%) increasingly benefited the growth of Fe-oxidizing *Am. ferrooxidans* ICP relative to S-oxidizing *At caldus* KU (Fig. 3b): This can be explained by the chemical catalytic role of activated carbon (details described in section 3.2), increasing the availability of  $\text{Fe}^{2+}$  ions for Fe-oxidizers while limiting the availability of RISCs for S-oxidizing cells. Since cell growth was significantly hindered at 0.3% activated carbon (Fig. 3a), the Real-Time PCR result was inconsistent under this particular condition (Fig. 3b).

### 3.2. $E_h$ -controlling mechanism of activated carbon (abiotic experiments)

In section 3.1, activated carbon was shown to control the  $E_h$  level during bioleaching of enargite concentrate. In order to clarify its catalytic mechanism, separate abiotic tests were performed.

In the presence of  $\text{Fe}^{3+}$  without any externally-added e-donors (such as  $\text{S}_4\text{O}_6^{2-}$  and yeast extract), a minor amount of initially-added  $\text{Fe}^{3+}$  was reduced to  $\text{Fe}^{2+}$  (0.6 mM;

Fig. 4a), accompanied by an  $E_h$  drop from 830 mV to 740 mV (Fig. 4b). In this case,  $\text{Fe}^{3+}$  reduction was likely coupled with oxidation of surface functional groups of activated carbon (Uchida et al., 2000).

When either  $\text{Fe}^{2+}$  or  $\text{S}_4\text{O}_6^{2-}$  solely contacted activated carbon, partial oxidation of each was observed (Fig. 4a, c), possibly directly by surface oxygen group or indirectly via reduction of oxygen to produce  $\text{H}_2\text{O}_2$  (Ahumada et al. 2002).

Progressive  $\text{Fe}^{3+}$  reduction to  $\text{Fe}^{2+}$  (9.2 mM; Fig. 4a) was realized only via the coupling reaction with  $\text{S}_4\text{O}_6^{2-}$  oxidation on the activated carbon surface (producing ~10 mM  $\text{SO}_4^{2-}$ ; Fig. 4c), showing the greatest  $E_h$ -lowering effect (down to ~620 mV; Fig. 4b). This effect was not as significant when yeast extract instead of  $\text{S}_4\text{O}_6^{2-}$  was used (Fig. 4b).

The above results indicate that activated carbon naturally possesses both  $\text{Fe}^{2+}$ -oxidizing and  $\text{Fe}^{3+}$ -reducing effects, which one of the two effects becomes visible depends on the availability of different functional groups and the degree of  $\text{H}_2\text{O}_2$  generation (Uchida et al., 2000; Ahumada et al., 2002). However, when strong e-donors (such as reduced inorganic sulfur compounds; RISCs) are present,  $\text{Fe}^{3+}$  reduction becomes dominant, leading to effective suppression of the  $E_h$  level. Although to a lesser extent, As(III) oxidation was also shown to be coupled with  $\text{Fe}^{3+}$  reduction on the activated carbon surface (Oyama et al., unpublished data). When elemental  $\text{S}^0$  was used as e-donor, the speed of  $\text{Fe}^{3+}$  reduction was seen but much slower (data not shown). This indicates that mainly soluble RISCs dissolved from sulfide minerals play a major role in this coupling reaction. These abiotic test results suggest that the presence of activated carbon plays a role to suppress the  $E_h$  level by catalyzing  $\text{Fe}^{3+}$  reduction using a series of RISCs produced in bioleaching situations (as well as organics and As(III), at least to some extent).

### 3.3. Galvanic interaction between enargite and activated carbon

To explain the catalytic mechanism of activated carbon, the involvement of

galvanic interaction between activated carbon and chalcopyrite during bioleaching has been suggested by other researchers (Nakazawa et al., 1998; Zhang et al., 2007; Liang et al., 2010). However, the actual occurrence of galvanic current between activated carbon and enargite is yet unclear. Fig. 5a shows that the electrode potential of pyrite ( $E_{Py}$ ) nearly equaled  $E_h$  at the wide  $E_h$  range of 0.5-0.85 V (Fig. 5a). However, the electrode potential of enargite ( $E_{En}$ ) and activated carbon ( $E_{Ac}$ ) mostly leveled off at  $E_h > 0.75$  V; this effect was especially significant with  $E_{En}$  (Fig. 5a). This indicates that the electromotive force generated between enargite and activated carbon ( $\Delta E_{En-Ac}$ ) is negligible at  $E_h < 0.75$  V, but increases slightly at  $E_h > 0.75$  V (Fig. 5a). Rather, the electromotive force generated between enargite and pyrite ( $\Delta E_{En-Py}$ ) was much more noticeable at  $E_h > 0.75$  V (Fig. 5a). This observation was indeed consistent with the trend of galvanic currents measured between enargite and activated carbon ( $I_{En-Ac}$ ) or between enargite and pyrite ( $I_{En-Py}$ ). Due to the greater  $\Delta E_{En-Py}$  than  $\Delta E_{En-Ac}$  at  $E_h > 0.75$  V,  $I_{En-Py}$  also exceeded  $I_{En-Ac}$  at the higher  $E_h$  values of  $> 0.75$  (Fig. 5b).

The overall results obtained here and previous sections suggest the following: Under the conditions where activated carbon displays the catalytic  $E_h$ -control ( $E_h < 700$  mV) during bioleaching, a relatively smaller galvanic effect is generated between enargite and activated carbon. While at higher  $E_h$  of  $> 750$  mV, the  $E_h$  level is no longer controlled by activated carbon but its galvanic interaction with enargite becomes relatively more significant than at  $E_h < 700$  mV. Nonetheless, the actual bioleaching results in Fig. 1 suggest that the overall Cu dissolution is governed mainly by the activated carbon's  $E_h$ -controlling effect rather than the galvanic effect under the conditions used in this study.

#### 3.4. Kinetic study on activated carbon-catalyzed bioleaching of enargite concentrate

The activated carbon-catalyzed bioleaching reactions (Fig. 1) were evaluated by the shrinking core model. The model was also effectively applied to the bioleaching

reaction of primary copper sulfides (Masaki et al., 2018; Oyama et al., 2018). Here the fluid film resistance was considered negligible relative to two others, and in fact, no linear relationships between  $X$  against  $t$  were found (data not shown). The  $k$  and  $R^2$  values were calculated from the fitting results and listed in Table 1.

The results from previous sections revealed that the main catalytic role of activated carbon in enargite bioleaching was  $\text{Fe}^{3+}$  reduction to control the  $E_h$  level ( $<700$  mV), which prolonged the period before initiation of extensive pyrite dissolution. For the period where  $E_h$  was controlled at  $<700$  mV, all bioleaching reactions were rate-limited by the surface chemical reaction ( $R^2 > 0.97$ ) regardless of the activated carbon dose. However, as soon as the  $E_h$  hits 700 mV, rapid pyrite dissolution was triggered to passivate the enargite surface to end the surface chemical reaction (Fig. 6a). Under the condition of  $E_h < 700$  mV, the speed of Cu dissolution (i.e., kinetic constant;  $k_r$  (day<sup>-1</sup>)) in bioleaching cultures became smaller as the activated carbon dose increased, with the fastest rate observed without activated carbon (Table 1; Fig. 6a). This is due to the dissolution of enargite mineral itself favors higher  $E_h$  (Lattanzi et al., 2008). Even so, the surface chemical reaction continued for a longer period at higher activated carbon doses, eventually reaching the greater final Cu dissolution in the longer-term (Fig. 6a).

#### 4. Conclusions

Although the enargite mineral itself favors higher  $E_h$  for solubilization, the dissolution of co-existing pyrite (also favors high  $E_h$ ) strongly inhibits the enargite dissolution through the passivation effect. Hence, when bioleaching the enargite concentrate (composed mainly of enargite and pyrite), the final Cu dissolution from the enargite mineral can be improved by allowing its successive and longer dissolution (though at a slower speed) under the controlled  $E_h$ . For this purpose, the catalytic effect



of activated carbon was found to become useful in bioleaching of enargite concentrate, as summarized in the proposed mechanism in Fig. 7:

(i) The activity of Fe-oxidizing microbes pushes the  $E_h$  level by regenerating  $Fe^{3+}$  in bioleaching cultures, which initially dissolve both enargite and pyrite minerals effectively, leading to a further increase in the  $E_h$  level. When activated carbon is absent, the dissolution of the enargite mineral becomes immediately hindered through the jarosite passivation.

(ii) When activated carbon is present, however, its surface effectively functions as an electron mediator to couple RISCs (especially soluble RISCs) oxidation and  $Fe^{3+}$  reduction, so that elevation of the  $E_h$  level can be offset. As long as the  $E_h$  level is suppressed at <700 mV, the dissolution of pyrite can be largely avoided, which allows a steady and continuous (but slower) dissolution of the enargite mineral through the surface chemical reaction model. Regeneration of  $Fe^{2+}$  by activated carbon may, however, support the activity of Fe-oxidizers. Consequently, when the  $E_h$ -control by activated carbon becomes no longer sustainable, the  $E_h$  hits 700 mV to initiate a rapid pyrite dissolution and the surface chemical reaction of the enargite mineral comes to end.

(iii) Since activated carbon also displays As(III) oxidation activity by coupling with  $Fe^{3+}$  reduction, this may partially contribute to the As precipitation in the form of amorphous ferric arsenate. However, when  $E_h$  level becomes no longer controllable after a while, the sudden initiation of pyrite dissolution triggered the re-solubilization of ferric arsenate by shifting the chemical equilibrium toward the formation of ferric sulfate such as jarosite.

The combination of the above reactions was shown to contribute to the activated carbon-catalyzed bioleaching of enargite concentrate. The sustainable  $E_h$ -controlling effect is thus critical to enable a longer Cu dissolution as well as stabilization of As precipitates.

## Reference

Ahonen, L. and Tuovinen, O.H., 1990. Catalytic effects of silver in the microbiological leaching of finely ground chalcopyrite-containing ore materials in shake flasks. *Hydrometallurgy* 24, 219-236.

Ahumada, E., Lizama, H., Orellana, F., Suárez, C., Huidobro, A., Sepúlveda-Escribano, A. and Rodriguez-Reinoso, F., 2002. Catalytic oxidation of Fe(II) by activated carbon in the presence of oxygen: Effect of the surface oxidation degree on the catalytic activity. *Carbon* 40, 2827-2834.

Anderson, I., Chertkov, O., Chen, A., Saunders, E., Lapidus, A., Nolan, M., Lucas, S., Hammon, N., Deshpande, S. and Cheng, J.-F., 2012. Complete genome sequence of the moderately thermophilic mineral-sulfide-oxidizing firmicute *Sulfobacillus acidophilus* type strain (NAL<sup>T</sup>). *Standards in Genomic Sciences* 6, 293.

Caldwell, D.H. and Adams, R.B., 1946. Colorimetric determination of iron in water with *o*-phenanthroline. *Journal of American Water Works Association* 38, 727-730.

Clum, A., Nolan, M., Lang, E., Del Rio, T.G., Tice, H., Copeland, A., Cheng, J., Lucas, S., Chen, F. and Bruce, D., 2009. Complete genome sequence of *Acidimicrobium ferrooxidans* type strain (ICP<sup>T</sup>). *Standards in Genomic Sciences* 1, 38.

Escobar, B., Huenupi, E. and Wiertz, J.V., 1997. Chemical and biological leaching of enargite. *Biotechnology Letters* 19, 719-722.

Escobar, B., Huenupi, E., Godoy, I. and Wiertz, J.V., 2000. Arsenic precipitation in the

bioleaching of enargite by *Sulfolobus* BC at 70 C. Biotechnology Letters 22, 205-209.  
 Ghahremaninezhad, A., Radzinski, R., Gheorghiu, T., Dixon, D.G. and Asselin, E., 2015.  
 A model for silver ion catalysis of chalcopyrite (CuFeS<sub>2</sub>) dissolution. Hydrometallurgy  
 155, 95-104.  
 Gu, G., Sun, X., Hu, K., Li, J. and Qiu, G., 2012. Electrochemical oxidation behavior of  
 pyrite bioleaching by *Acidithiobacillus ferrooxidans*. Transactions of Nonferrous Metals  
 Society of China 22, 1250-1254.  
 Hao, X., Liu, X., Zhu, P., Chen, A., Liu, H., Yin, H., Qiu, G. and Liang, Y., 2018. Carbon  
 material with high specific surface area improves complex copper ores' bioleaching  
 efficiency by mixed moderate thermophiles. Minerals 8, 301.  
 Hiroyoshi, N., Arai, M., Miki, H., Tsunekawa, M. and Hirajima, T., 2002. A new reaction  
 model for the catalytic effect of silver ions on chalcopyrite leaching in sulfuric acid  
 solutions. Hydrometallurgy 63, 257-267.  
 Hiroyoshi, N., Tsunekawa, M., Okamoto, H., Nakayama, R., Kuroiwa, S., 2008.  
 Improved chalcopyrite leaching through optimization of redox potential. Canadian  
 Metallurgical Quarterly 47, 253–258.  
 Jahromi, F. and Ghahreman, A., 2016. Activated carbon assisted atmospheric leaching of  
 enargite in chloride media, International Copper Conference 2016 Abstract, pp. 1453-  
 1464.

Jahromi, F.G. and Ghahreman, A., 2018. In-situ oxidative arsenic precipitation as scorodite during carbon catalyzed enargite leaching process. Journal of Hazardous Materials 360, 631-638.

Jahromi, F.G., Alvial-Hein, G., Cowan, D.H. and Ghahreman, A., 2019. The kinetics of enargite dissolution in chloride media in the presence of activated carbon and AF 5 catalysts. Minerals Engineering 143, 106013.

Konadu, K.T., Sasaki, K., Kaneta, T., Ofori-Sarpong, G. and Osseo-Asare, K., 2017. Bio-modification of carbonaceous matter in gold ores: Model experiments using powdered activated carbon and cell-free spent medium of *Phanerochaete chrysosporium*. Hydrometallurgy 168, 76-83.

Lattanzi, P., Da Pelo, S., Musu, E., Atzei, D., Elsener, B., Fantauzzi, M. and Rossi, A., 2008. Enargite oxidation: A review. Earth-Science Reviews 86, 62-88.

Lee, J., Acar, S., Doerr, D.L. and Brierley, J.A., 2011. Comparative bioleaching and mineralogy of composited sulfide ores containing enargite, covellite and chalcocite by mesophilic and thermophilic microorganisms. Hydrometallurgy 105, 213-221.

Li, B., Chen, Y., Liu, Q., Hu, S. and Chen, X., 2011. Complete genome analysis of *Sulfobacillus acidophilus* strain TPY, isolated from a hydrothermal vent in the Pacific Ocean. Journal of Bacteriology 193, 5555-5556.

Liang, C., Xia, J., Zhao, X., Yang, Y., Gong, S., Nie, Z., Ma, C., Zheng, L., Zhao, Y. and Qiu, G., 2010. Effect of activated carbon on chalcopyrite bioleaching with extreme

thermophile *Acidianus manzaensis*. Hydrometallurgy 105, 179-185.

Ma, Y., Liu, H., Xia, J., Nie, Z., Zhu, H., Zhao, Y., Zheng, L., Hong, C. and Wen, W., 2017. Relatedness between catalytic effect of activated carbon and passivation phenomenon during chalcopyrite bioleaching by mixed thermophilic Archaea culture at 65°C. Transactions of Nonferrous Metals Society of China 27, 1374-1384.

Masaki, Y., Hirajima, T., Sasaki, K., Miki, H. and Okibe, N., 2018. Microbiological redox potential control to improve the efficiency of chalcopyrite bioleaching. Geomicrobiology Journal 35, 648-656.

Miki, H., Iguchi, A., Hirajima, T. and Sasaki, K., 2016. Catalytic effect of silver on arsenic-containing copper sulfide dissolution in acidic solution. Hydrometallurgy 162, 1-8.

Muñoz, J., Blázquez, M., González, F., Ballester, A., Acevedo, F., Gentina, J. and González, P., 2006. Electrochemical study of enargite bioleaching by mesophilic and thermophilic microorganisms. Hydrometallurgy 84, 175-186.

Muñoz, J., Dreisinger, D., Cooper, W. and Young, S., 2007. Silver-catalyzed bioleaching of low-grade copper ores: Part I: Shake flasks tests. Hydrometallurgy 88, 3-18.

Nakazawa, H., Fujisawa, H. and Sato, H., 1998. Effect of activated carbon on the bioleaching of chalcopyrite concentrate. International Journal of Mineral Processing 55, 87-94.

Nazari, G., Dixon, D. and Dreisinger, D., 2011. Enhancing the kinetics of chalcopyrite leaching in the Galvanox™ process. *Hydrometallurgy* 105, 251-258.

Nazari, G., Dixon, D. and Dreisinger, D., 2012a. The role of silver-enhanced pyrite in enhancing the electrical conductivity of sulfur product layer during chalcopyrite leaching in the Galvanox™ process. *Hydrometallurgy* 113, 177-184.

Nazari, G., Dixon, D. and Dreisinger, D., 2012b. The mechanism of chalcopyrite leaching in the presence of silver-enhanced pyrite in the Galvanox™ process. *Hydrometallurgy* 113, 122-130.

Okibe, N., Fukano, Y., 2019. Bioremediation of highly toxic arsenic via carbon-fiber-assisted indirect As(III) oxidation by moderately-thermophilic, acidophilic Fe-oxidizing bacteria. *Biotechnology Letters* 41, 1403–1411

Olvera, O., Dixon, D. and Asselin, E., 2013. Electrochemical study of the dissolution of enargite (Cu<sub>3</sub>AsS<sub>4</sub>) in contact with activated carbon. *Electrochimica Acta* 107, 525-536.

Oyama, K., Shimada, K., Ishibashi, J., Miki, H. and Okibe, N., 2018. Silver-catalyzed bioleaching of enargite concentrate using moderately thermophilic microorganisms. *Hydrometallurgy* 177, 197-204.

Sasaki, K., Takatsugi, K., Kaneko, K., Kozai, N., Ohnuki, T., Tuovinen, O. and Hirajima, T., 2010. Characterization of secondary arsenic-bearing precipitates formed in the bioleaching of enargite by *Acidithiobacillus ferrooxidans*. *Hydrometallurgy* 104, 424-431.

Takatsugi, K., Sasaki, K. and Hirajima, T., 2011. Mechanism of the enhancement of bioleaching of copper from enargite by thermophilic iron-oxidizing archaea with the concomitant precipitation of arsenic. *Hydrometallurgy* 109, 90-96.

Tanaka, M., Sasaki, K. and Okibe, N., 2018. Behavior of sulfate ions during biogenic scorodite crystallization from dilute As(III)-bearing acidic waters. *Hydrometallurgy* 180, 144-152.

Tanaka, M., Yamaji, Y., Fukano, Y., Shimada, K., Ishibashi, J.-I., Hirajima, T., Sasaki, K., Sawada, M. and Okibe, N., 2015. Biooxidation of gold-, silver, and antimony-bearing highly refractory polymetallic sulfide concentrates, and its comparison with abiotic pretreatment techniques. *Geomicrobiology Journal* 32, 538-548.

Travisany, D., Di Genova, A., Sepúlveda, A., Bobadilla-Fazzini, R.A., Parada, P. and Maass, A., 2012. Draft genome sequence of the *Sulfobacillus thermosulfidooxidans* Cutipay strain, an indigenous bacterium isolated from a naturally extreme mining environment in Northern Chile. *Journal of Bacteriology* 194, 6327-6328.

Uchida, M., Shinohara, O., Ito, S., Kawasaki, N., Nakamura, T. and Tanada, S., 2000. Reduction of iron(III) ion by activated carbon fiber. *Journal of Colloid and Interface Science* 224, 347-350.

Valdes, J., Quatrini, R., Hallberg, K., Dopson, M., Valenzuela, P.D. and Holmes, D.S., 2009. Draft genome sequence of the extremely acidophilic bacterium *Acidithiobacillus caldus* ATCC 51756 reveals metabolic versatility in the genus *Acidithiobacillus*. *Journal of Bacteriology* 191, 5877-5878.

Zhang, W. and Gu, S., 2007. Catalytic effect of activated carbon on bioleaching of low-grade primary copper sulfide ores. Transactions of Nonferrous Metals Society of China 17, 1123-1127.

## Legends

### Fig. 1

Bioleaching of enargite concentrate using different dose of activated carbon (○● 0%; ▲ 0.1%; ▼ 0.2%; □■ 0.3%). Changes in the dissolved Cu concentration (a), dissolved Fe concentration (b), dissolved As concentration (c),  $E_h$  (d),  $Fe^{2+}$  concentration (e) and immobilized As concentration (f) are shown for inoculated (solid symbols) or cell-free control cultures (open symbols). Data points in (f) were calculated based on the chemical formula of enargite ( $Cu_3AsS_4$ ) as follows;  $[As \text{ immobilized}] \text{ (mM)} = [Cu \text{ dissolved}]/3 \text{ (mM)} - [As \text{ dissolved}] \text{ (mM)}$ . Dotted lines in (a), (b), (d) and (f) indicate the timing of the  $E_h$  level reaching 700 mV. Data points are mean values from duplicate cultures. Error bars depicting averages are not visible in some cases as they are smaller than the data point symbols.

### Fig. 2

EPMA elemental mapping of enargite concentrate residue bioleached for 30 days with 0.2% activated carbon: The backscattered electron image at 3000-fold magnification (a) was mapped for Cu (b), S (c), Fe (d), As (e) and O (f). The surface of an enargite grain (middle) is covered with Fe-, As-, O-containing amorphous ferric arsenate.



**Fig. 3**

Changes in the planktonic cell density during bioleaching of enargite concentrate at different dose of activated carbon (AC) (●: 0%, ▲: 0.1%, ▼: 0.2%, ■: 0.3%) (a) and the microbial population structures on day 30 and 60 under each condition (b). Data points in (a) are mean values from duplicate cultures. Error bars depicting averages are not visible in some cases as they are smaller than the data point symbols. KU, ICP and N1 stand for *At. caldus* KU, *Am. ferrooxidans* ICP and *Sb. sibiricus* N1, respectively.

**Fig. 4**

Chemical  $\text{Fe}^{3+}$ -reducing ability of activated carbon (AC) using  $\text{S}_4\text{O}_6^{2-}$  as electron donor. Changes in the  $\text{Fe}^{2+}$  concentration (a),  $E_h$  (b) and  $\text{SO}_4^{2-}$  concentration (c) are shown for the following conditions: ▲ ; AC+ $\text{Fe}^{3+}$ , ▼ ; AC+ $\text{Fe}^{2+}$ , ◆ ; AC+ $\text{S}_4\text{O}_6^{2-}$ , ■ ; AC+ $\text{Fe}^{3+}$ + $\text{S}_4\text{O}_6^{2-}$ , × ; AC+ $\text{Fe}^{3+}$ +yeast extract (YE), ● ;  $\text{Fe}^{3+}$ + $\text{S}_4\text{O}_6^{2-}$ . Data points are mean values from duplicate cultures. Error bars depicting averages are not visible in some cases as they are smaller than the data point symbols.

**Fig. 5**

(a) Mineral electrode potential of enargite (●), pyrite (■) or activated carbon (AC) (◇) as the function of solution potential ( $E_h$ ): △ indicates the amount of Galvanic electromotive force created between activated carbon and enargite/pyrite. (b) Galvanic current created between enargite and pyrite (■) or between enargite and activated carbon (◇), as the function of solution potential ( $E_h$ ). The grey zone indicates the  $E_h$  range exhibited during the separate bioleaching test (Fig. 1d).

**Fig. 6**

Kinetic modeling on bioleaching of enargite concentrate at different activated carbon doses: 0% (●), 0.1% (▲), 0.2% (▼) or 0.3% (■). Bioleaching data in Fig. 1 were applied. (a) Data fitted to the surface chemical reaction model ( $1 - (1-X)^{1/3} = k_{rt}t$ ). (b) Data fitted to the diffusion through product film model ( $1 + 2(1-X) - 3(1-X)^{2/3} = k_{dt}t$ ). The fitting duration for each condition corresponds to the period before  $E_h$  reaching 700 mV (i.e., before initiation of rapid pyrite dissolution), after which the  $R^2$  value started to decrease in all cases. Solid and dotted lines indicate  $R^2 > 0.97$  and  $R^2 < 0.93$ , respectively.

## Fig. 7

The schematic image of overall mechanism of activated carbon-catalyzed bioleaching of enargite concentrate.

## Table 1

Correlation factor  $R^2$  and kinetic constant  $k$  values calculated using the kinetic model of surface chemical reaction and diffusion through product film.

## Supplemental Fig. 1

Changes in the pH in bioleaching (closed symbol) and cell-free control cultures (open symbol) of enargite concentrate. Activated carbon was added at 0% (○, ●), 0.1% (▲), 0.2% (▼), or 0.3% (□, ■). Data points are mean values from duplicate cultures. Error bars depicting averages are not visible in some cases as they are smaller than the data point symbols.

## Acknowledgements

This work was partly supported by JSPS KAKENHI Grant Number JP20H00647.

Enargite concentrate was kindly provided by JX Nippon Mining & Metals. K. O. is

617 grateful for financial support provided by the Kyushu University Advanced Graduate  
618 Program in Global Strategy for Green Asia.